Optical and Quantum Electronics **33:** 315–325, 2001.

A fully vectorial technique for scattering and propagation in three-dimensional stratified photonic structures

MICHAEL PAULUS[1,2] AND OLIVIER J.F. MARTIN[1]*
[1]*Electromagnetic Fields and Microwave Electronics Laboratory, Swiss Federal Institute of Technology, ETH-Zentrum ETZ, CH-8092 Zurich, Switzerland*
[2]*IBM Research Division, Zurich Research Laboratory, CH-8803 Rüschlikon, Switzerland*
*(*author for correspondence: E-mail: martin@ifh.ee.ethz.ch)*

Abstract. We present a three-dimensional (3D) technique for computing light scattering and propagation in complex structures formed by scatterers embedded in a stratified background. This approach relies on the Green's tensor associated with the background and requires only the discretization of the scatterers, the entire stratified background being accounted for in the Green's tensor. Further, the boundary conditions at the edges of the computation window and at the different material interfaces in the stratified background are automatically fulfilled. Different examples illustrate the application of the technique to the modeling of photonic integrated circuits: waveguides with protrusions (single element 'grating') and notches. Subtle effects, like polarization crosstalks in an integrated optics device are also investigated.

Key words: computational technique, eigenmodes, Green's tensor, integrated optics, light propagation, polarization, scattering, stratified media, waveguides

1. Introduction

Most photonic integrated circuits (PICs) are built on a stratified background. This background, formed by a stack of layers with different permittivities, is used to confine and guide the light. The particular functions in the circuit (light source, switch, coupler, modulator, detector, etc.) are then incorporated as distinct components in this background (e.g., a quantum well in a stratified laser structure or a grating on top of a waveguide).

Different approaches can be used for the simulation of such PICs, for example eigenmode expansions (Herzinger *et al.* 1993; Willems *et al.* 1995; Derudder *et al.* 1998), finite difference time domain algorithms (Lee *et al.* 1992; Hayes *et al.* 1999), finite element methods (Davies 1993; Noble *et al.* 1998), beam propagation methods (Huang and Xu 1993; Hsueh *et al.* 1999; El-Refaei *et al.* 2000) or the method of lines (Helfert and Pregla 1999; Huang and Syms 1999). For a recent review, see e.g., Scarmozzino *et al.* (2000).

We recently proposed a new approach to this problem, based on the Green's tensor technique (Paulus and Martin 2001). It is a fully vectorial

model for three-dimensional (3D) structures based on the solution of the electric field integral equation. We will briefly outline this technique in Section 2 and illustrate in Section 3 its application to several 3D integrated optics systems. We will summarize our results in Section 4.

2. The Green's tensor technique

We consider a system formed by distinct 3D scatterers with permittivity $\varepsilon(\mathbf{r})$ embedded in a stratified background made up of L material layers with permittivities $\varepsilon_i, i = 1, \ldots, L$ (Fig. 1(a)). Throughout this paper, we consider non-magnetic materials ($\mu = 1$) and assume a harmonic time dependence $\exp(-i\omega t)$ for the fields.

The core of our technique is the integral equation for the electric field,

$$\mathbf{E}(\mathbf{r}) = \mathbf{E}^0(\mathbf{r}) + \int_V d\mathbf{r}' \mathbf{G}(\mathbf{r}, \mathbf{r}') \cdot k_0^2 \Delta\varepsilon(\mathbf{r}') \mathbf{E}(\mathbf{r}'), \tag{1}$$

which gives the total scattered field $\mathbf{E}(\mathbf{r})$ when the system is illuminated with an incident field $\mathbf{E}^0(\mathbf{r})$ propagating in the stratified background (Tai 1994; Martin and Piller 1998).

In Equation (1), $k_0 = \omega/c$ is the wave number in vacuum; the dielectric contrast $\Delta\varepsilon(\mathbf{r})$ represents the polarizability of the scatterer compared to that of the background and is defined by

$$\Delta\varepsilon(\mathbf{r}) = \varepsilon(\mathbf{r}) - \varepsilon_\kappa \quad \text{for } \mathbf{r} \in \text{layer } \kappa. \tag{2}$$

The tensor $\mathbf{G}(\mathbf{r}, \mathbf{r}')$ is the Green's tensor associated with the stratified background. It contains the entire response of the stratified background and includes all reflections/refractions at any interface, as well as the radiation conditions at infinity.

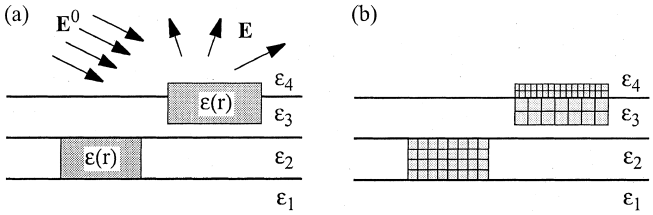

Fig. 1. (a) Typical structure under study: a stratified background formed by L layers of materials with different permittivities ε_i contains several scatterers $\varepsilon(\mathbf{r})$. The structure is illuminated with an incident field $\mathbf{E}^0(\mathbf{r})$ and our objective is to compute the total field $\mathbf{E}(\mathbf{r})$ in the system. Note that the first and last background layers represent semi-infinite media. (b) Only the scatterers must be discretized to solve the scattering problem numerically using the Green's tensor technique. A non-regular mesh, with higher refinement in the regions of high contrast is used.

This dyadic cannot be obtained analytically and must be computed numerically. This is best achieved by expressing $\mathbf{G}(\mathbf{r}, \mathbf{r}')$ in Fourier space and using the symmetry properties of the stratified background in that space. We recently detailed this procedure in Paulus *et al.* (2000) and refer the reader to this publication. In the present article, we will simply use $\mathbf{G}(\mathbf{r}, \mathbf{r}')$ to perform scattering calculations with Equation (1).

However, before doing so, we would like to illustrate the physical signification of the Green's tensor for a stratified background: for a given source–observer $\mathbf{r}', \mathbf{r}$ pair, the 3×3 matrix representing the Green's tensor,

$$\mathbf{G}(\mathbf{r}, \mathbf{r}') = \begin{pmatrix} G_{xx} & G_{xy} & G_{xz} \\ G_{yx} & G_{yy} & G_{yz} \\ G_{zx} & G_{zy} & G_{zz} \end{pmatrix}, \tag{3}$$

gives the electric field radiated at $\mathbf{r}$ by three orthogonal dipoles located at $\mathbf{r}'$.

For example, Fig. 2 illustrates the first column of $\mathbf{G}(\mathbf{r}, \mathbf{r}')$, corresponding to the three components of the electric field radiated by an x-oriented dipolar source. The source point is located at $\mathbf{r}' = (0, 0, 250\,\text{nm})$ in the stratified background corresponding to Fig. 3. The wavelength is $\lambda = 633\,\text{nm}$ (note that in Section 3 we consider a wavelength $\lambda = 1.55\,\mu\text{m}$). The three components of the Green's tensor are computed along a vertical line in the stratified background, at a one wavelength lateral distance from the source point. One notices in Fig. 2 that both in the cap InP layer and in the InGaAsP layer, the electric field oscillates in a manner that corresponds to a stationary wave

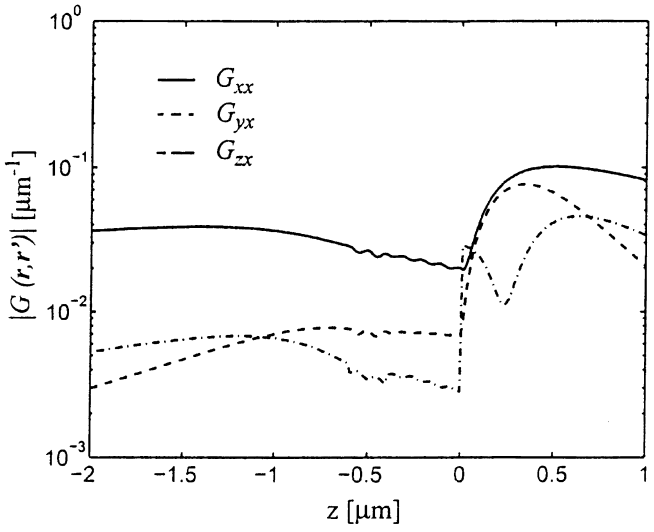

Fig. 2. Three components of the Green's tensor for the stratified background corresponding to the structure depicted in Fig. 3.

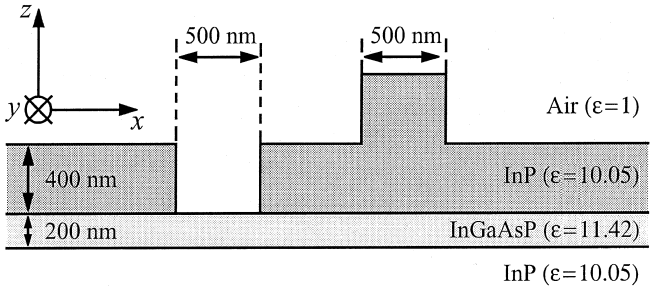

Fig. 3. Geometry and permittivity of the system: a notch is etched in, or a protrusion deposited on top of an InP/InGaAsP structure. The structure is illuminated with a TE_0 or a TM_0 mode propagating in x-direction and the scattered field is computed.

excited in the corresponding layer, with a shorter effective wavelength in the layer with the highest index (InGaAsP). The x and y electric field components are parallel to the interfaces and therefore continuous. On the other hand, the z component is normal to the material interfaces and therefore discontinuous, as is visible in Fig. 2. This figure illustrates the significant physical information contained in the Green's tensor.

To solve Equation (1) numerically, we define a mesh on the system with N discretized elements centered at $\mathbf{r}_i$ with permittivity $\varepsilon_i = \varepsilon(\mathbf{r}_i)$ and volume V_i (Fig. 1(b)). The discretization volume V_i need not be constant and, in order to achieve a given accuracy, it is actually necessary to use a smaller mesh where the dielectric contrast is larger (Piller and Martin 1998). Each mesh must be entirely inside a layer and cannot sit astride a boundary between two layers (Fig. 2(b)).

We can formally write the discretized system of equations corresponding to Equation (1):

$$\mathbf{E}_i = \mathbf{E}_i^0 + \sum_{j=1}^{N} \mathbf{G}_{i,j} \cdot k_0^2 \, \Delta\varepsilon_j \mathbf{E}_j V_j, \quad i = 1, \ldots, N. \tag{4}$$

It should be noted that a special treatment must be applied to the case $j = i$ since the Green's tensor diverges in that case. This procedure, which is detailed in Paulus and Martin (2001), leads to additional terms in Equation (4).

The system of Equations (4) is then solved numerically, e.g. with an iterative solver, to obtain the unknown discretized field $\mathbf{E}_i$ for a given illumination $\mathbf{E}^0$.

Let us finally note that Equation (1) can also be used for scattering calculations in an infinite homogeneous background (instead of a stratified background) by simply using the corresponding Green's tensor. In that case, $\mathbf{G}(\mathbf{r}, \mathbf{r}')$ takes a very simple analytical form (Martin and Piller 1998).

3. Results

To illustrate this technique, we consider the InP/InGaAsP waveguide structure depicted in Fig. 3. At the wavelength of 1.55 μm, the InGaAsP guide can support two different modes: a transverse electric TE_0 mode, with the electric field polarized in the y-direction, and a transverse magnetic TM_0 mode, with the electric field in the (x, z)-plane.

Fig. 4 gives the total electric field amplitude (square root of $\mathbf{E} \cdot \mathbf{E}^*$) when the system is illuminated with a TE_0 mode propagating in the x-direction. An InP protrusion has been deposited on the structure. This single step 'grating' somewhat disturbs the propagation of the mode, leading to light scattered into the substrate. The interaction of this scattered light with the incident field produces an interference pattern on the left-hand side of the protrusion in Fig. 4(a). The diffraction of the incoming mode is particularly visible in the middle of the InGaAsP layer, where a depletion in the field amplitude appears just behind the protrusion (Fig. 4(b), note that the gray-scale is chosen to emphasize the structure of the field distributions, leading to different saturation values for the distribution in a (x, z)- or a (x, y)-plane). However, due to the limited lateral extension of the protrusion, this scattering effect remains localized and, quite rapidly, the incident mode is re-established in the structure. A similar behavior is observed when a TM_0 illumination is used (not shown).

Let us point out how perfectly the boundary conditions at the edges of the computation window and at the interface between the different layers are fulfilled. This at no additional computational costs, since these complex boundary conditions are already included in the Green's tensor $\mathbf{G}(\mathbf{r}, \mathbf{r}')$.

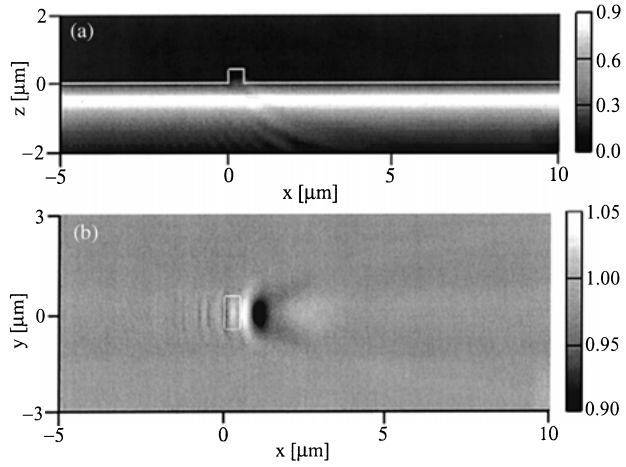

Fig. 4. Total field amplitude when a $x = 500\,\text{nm}, y = 1\,\mu\text{m}$ and $z = 400\,\text{nm}$ InP protrusion is deposited on the structure. TE_0 illumination. (a) Side view ($y = 0$), (b) top view ($z = -550\,\text{nm}$, the projection of the protrusion is shown).

The scattering increases when a second protrusion is deposited on the structure (Fig. 5). The field amplitude just inside the protrusion is now somewhat larger than in the case of a single protrusion. This field is the forerunner of the field that will be diffracted off the structure when a longer grating is deposited on the surface (Hunsperger 1991; März 1994). The light intensity diffused into the substrate also increases slightly, while the interaction of the field scattered by the two protrusions produces a more complex pattern inside the waveguide (Fig. 5(b)).

Since our approach is fully 3D, we can position protrusions on the structure arbitrarily, as illustrated in Fig. 6. In that case of two protrusions with a lateral offset, a fairly complex field distribution appears inside the waveguide. This pattern depends on the mode that is used to illuminate the structure: for TE_0 illumination, the field in the waveguide reaches a maximum just after each protrusion, followed by a field minimum (Fig. 6(a)). For TM_0 illumination, the diffraction pattern is broader, with a maximum field amplitude inside the protrusion (Fig. 6(b)). The interference pattern resulting from the interaction of the field scattered by the different elements is particularly visible for TM_0 polarization (Fig. 6(b)). Striking on that figure is the difference in the periodicity of the field in the forward direction and in the backward direction, the former being related to the interference of the light scattered by the protrusions and the latter being related to the 'stationary wave' resulting from the interaction of the incident field with the back-scattered field.

The difference of behavior observed in Fig. 6 for TE_0 and TM_0 excitations can be related to the different boundary conditions experienced by the electric field, depending on its orientation relative to the protrusion boundaries (Martin *et al.* 1994). A quantitative comparison of the scattering amplitudes

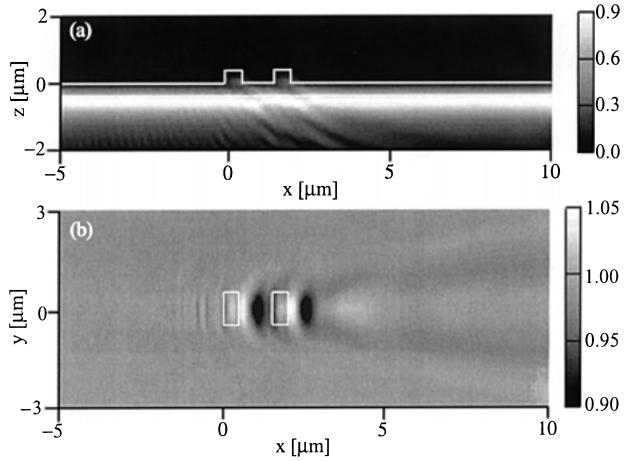

Fig. 5. Same situation as in Fig. 4 but with two similar protrusions.

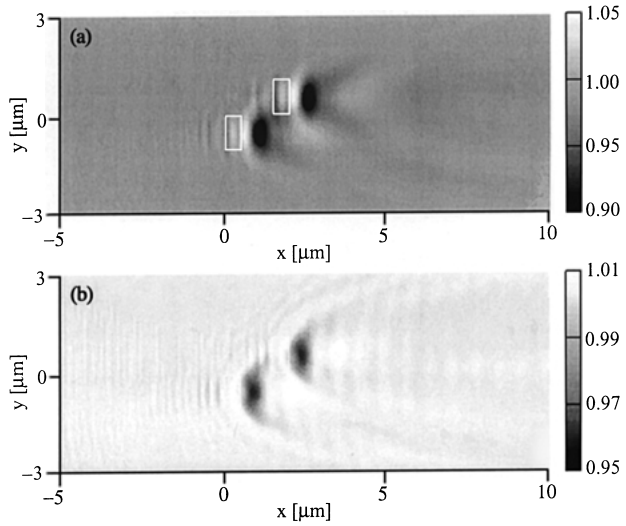

Fig. 6. Same situation as in Fig. 4 but with two protrusions offset in y-direction. The field is computed in the guiding layer ($z = -550$ nm) and the projection of the protrusions is shown: (a) TE_0 illumination and (b) TM_0 illumination.

shows that the interaction with the protrusion is stronger for the TE_0 mode than for the TM_0 mode.

The different scatterers placed in the background do not need to be aligned in a particular direction, as illustrated in Fig. 7, where the situation is similar to that of Fig. 6, but with a tilted protrusion. The scatterers can also extend over several background layers. This direct space discretization is therefore extremely versatile and can handle a broad range of physical systems.

A more dramatic effect on the guided wave is observed when a notch is etched inside the cap InP layer, as depicted in Fig. 8. Note that for this simulation the dielectric contrast $\Delta\varepsilon$ in Equation (1) is negative since the scatterer permittivity (air, $\varepsilon = 1$) is smaller than the permittivity of its surrounding layer (InP).

An important part of the incident TE_0 field is now scattered into the substrate (Fig. 8(b)). The back-scattered field is also larger, producing a marked interference pattern in the waveguide and in the substrate. Further, within the simulation window, the incident mode does not re-establish in the forward direction with the same intensity (compare Fig. 8(b) with Fig. 4(b)).

As a last example, we would like to briefly discuss the polarization coupling that can occur in the waveguide structure investigated in Fig. 8. Since our approach is fully vectorial, the electric field computed using Equation (1) includes all three components, even when the excitation $\mathbf{E}^0$ is only a scalar field. As an example, in Fig. 9(a), we consider a TE_0 incident field, i.e., an incident field with only a y-component. However, during the scattering process, a TM electric field, with x- and z-components, is generated.

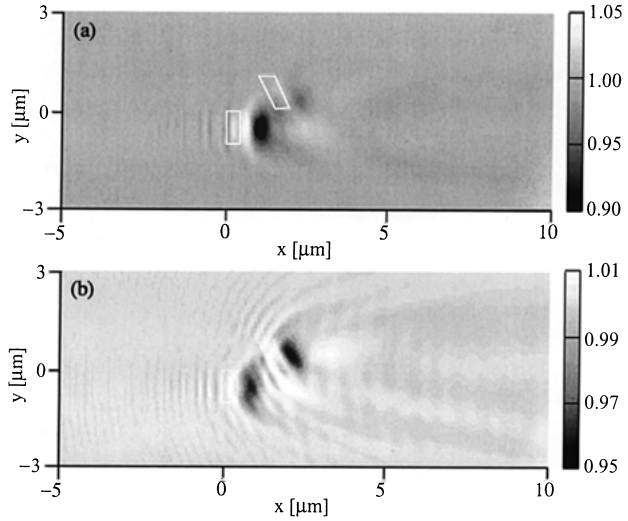

Fig. 7. Same situation as in Fig. 6, but now with one tilted protrusion. The field is computed in the guiding layer ($z = -550$ nm) and the projection of the protrusions is shown: (a) TE_0 illumination and (b) TM_0 illumination.

Its amplitude is represented in Fig. 9(a). Note the perfect symmetry of this field, related to the fact that the scatterer is symmetrical and the incident field propagates along one of its symmetry axis. The interference pattern in Fig. 9(a) originates from the finite extension of the scatterer (in the order of one wavelength). This interference pattern is similar in the forward and backward directions. This is because no TM components were present in the

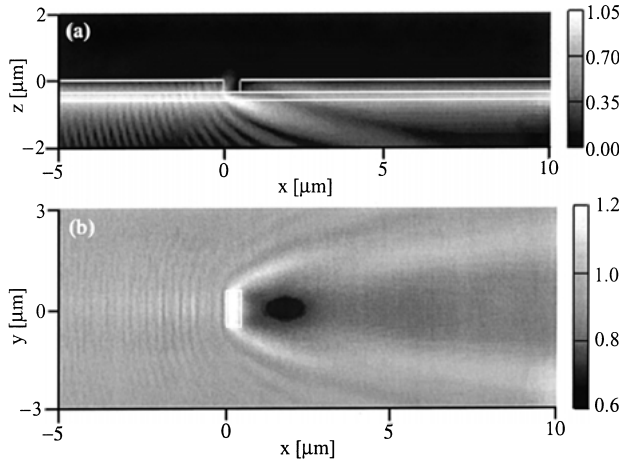

Fig. 8. Same situation as in Fig. 4 but now a notch with similar dimensions is etched through the InP layer.

incident field. Therefore no interferences between incident and reflected field can occur for this polarization component (compare with Fig. 8(a)).

A similar effect is observed when a notch is etched in the waveguide (Fig. 9(b)). For that geometry, the interaction is stronger and the amplitude of the TM field created during the scattering process is larger (notice the different amplitude scales in Fig. 9(a) and (b)).

Fig. 10 shows for the case of a waveguide with a notch (Fig. 9(b)) the real part of electric field components created during the scattering process: the z-component for a TE_0 incident field and the y-component for a TM_0 incident field.

These new field components correspond to a field generated at the location of the notch and propagating in both directions in the waveguide. A mode cross-polarized to the incident field is therefore established in the waveguide. As a matter of fact, an analysis of the generated field shows that its propagation constant is identical to the propagation constant which can be expected for a mode of that polarization (Fig. 10). Note however that the amplitude of this cross-polarized mode is much smaller than the amplitude of the original incident field. For the geometry of Fig. 9(a) (protrusion) a

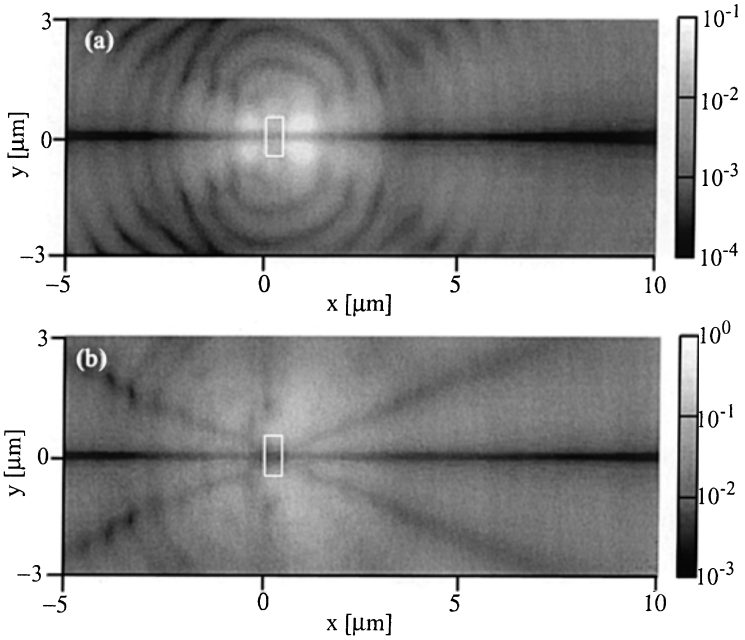

Fig. 9. (a) Same geometry as in Fig. 4; the field in the guiding layer ($z = -550\,\text{nm}$) is shown. The waveguide is excited with a TE_0 mode and the amplitude of the TM field is computed; this polarization, which was not present in the excitation, is created during the scattering process. (b) Same situation but with a notch (as in Fig. 8) instead of a protrusion. Note that in both figures a different logarithmic grayscale is used.

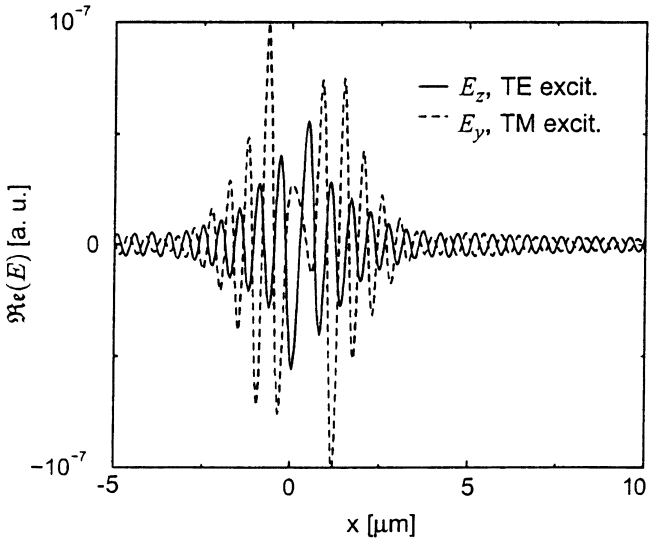

Fig. 10. Real part of the electric field components created during the scattering process depicted in Fig. 9(b) (notch): E_z, respectively E_y, are shown for a TE_0, respectively TM_0, excitation of the structure. These new field components, that were not present in the illumination field, are shown along the center of the structure ($y = 0$ in Fig. 9(b)).

similar behavior could not be observed because the perturbation of the incident field by the protrusion is not strong enough to generate a cross-polarized mode.

4. Conclusion

We have presented a fully vectorial 3D technique, based on the Green's tensor, for scattering computations in stratified media. In this approach, only the elements that differ from the stratified background must be discretized; the response of the background being taken into account by the Green's tensor. Further, the boundary conditions at the edges of the computation window, as well as at the different interfaces in the stratified background are automatically fulfilled.

The different examples presented have illustrated the versatality of this approach and its suitability for investigating subtle effects such as polarization crosstalks in a waveguide.

We believe that this technique can handle a broad range of complex systems, including integrated optical circuits and photonic band gap structures. However, since it is a fully 3D vectorial approach, the computational costs can become prohibitive for very large systems.

Acknowledgements

We thank B. Michel and R. Vahldieck for their support of the project and gratefully acknowledge funding of the Swiss National Science Foundation.

References

Davies, J.B. *IEEE Trans. Magn.* **29** 1578, 1993.
Derudder, H., D. De Zutter and F. Olyslager. *Electron. Lett.* **34** 2138, 1998.
El-Refaei, H., D. Yevick and I. Betty. *IEEE Photon. Tech. L.* **12** 389, 2000.
Hayes, P.R., M.T. O'Keefe, P.R. Woodward and A. Gopinath. *Opt. Quant. Electron.* **31** 813, 1999.
Helfert, S.F. and R. Pregla. *Opt. Quant. Electron.* **31** 721, 1999.
Herzinger, C.M., C.C. Lu, T.A. DeTemple and W.C. Chew. *IEEE J. Quant. Electron.* **29** 2273, 1993.
Hsueh, Y., M. Yang and H. Chang. *J. Lightwave Technol.* **17** 2389, 1999.
Huang, W. and R.R.A. Syms. *J. Lightwave Technol.* **17** 2658, 1999.
Huang, W.P. and C.L. Xu. *IEEE J. Quant. Electron.* **29** 2639, 1993.
Hunsperger, R.G. *Integrated Optics: Theory and Technology* 3rd edn, Springer, Berlin, 1991.
Lee, J.-F., R. Palandech and R. Mittra. *IEEE Trans. Microwave Theory Technol.* **40** 346, 1992.
Martin, O.J.F., A. Dereux and C. Girard. *J. Opt. Soc. Am. A* **11** 1073, 1994.
Martin, O.J.F. and N.B. Piller. *Phys. Rev. E* **58** 3909, 1998.
März, R. *Integrated Optics Design and Modeling*. Artech House, Boston, 1994.
Noble, M.J., J.A. Lott and J.P. Loehr. *IEEE J. Quant. Electron.* **34** 2327, 1998.
Paulus, M., P. Gay-Balmaz and O.J.F. Martin. *Phys. Rev. E* **62** 5797, 2000.
Paulus, M. and O.J.F. Martin. *J. Opt. Soc. Am. A.* **18** 854, 2001.
Piller, N.B. and O.J.F. Martin. *IEEE Trans. Antennas Propag.* **46** 1126, 1998.
Scarmozzino, R., A. Gopinath, R. Pregla and S. Helfert. *IEEE J. Sel. Top. Quant.* **6** 150, 2000.
Tai, C.-T. *Dyadic Green Function in Electromagnetic Theory*. IEEE Press, New York, 1994.
Willems, J., J. Haes and R. Baets. *Opt. Quant. Electron.* **27** 995, 1995.